Scintillation and storage luminescence properties of MgF$_2$ transparent ceramics doped with Ce^{3+}

Fumiya Nakamura [a], [*], Takumi Kato [a], Go Okada [a], Noriaki Kawaguchi [a], Kentaro Fukuda [b], Takayuki Yanagida [a]

[a] Nara Institute of Science and Technology (NAIST), 8916-5 Takayama-cho, Ikoma-shi, Nara, 630-0192, Japan
[b] Tokuyama Corporation, 1-1 Mikage-cho, Shunan-shi, Yamaguchi, 745-8648, Japan

ARTICLE INFO

ABSTRACT

In this paper, we report basic optical properties and scintillation and storage luminescence properties of MgF$_2$:Ce transparent ceramics with different doping concentrations of Ce (0.01, 0.1 and 1%) synthesized by spark plasma sintering (SPS). In scintillation, thermally-stimulated luminescence (TSL) and optically-stimulated luminescence (OSL), the dominant emissions were due to the 5d-4f transitions of Ce^{3+} which appeared in the near-UV region peaking around 320 and 360 nm. The scintillation was evaluated by X-ray irradiation while OSL was observed under 540 nm stimulation. In particular, the TSL sensitivity was high and showed a good linearity from 0.1 mGy to 1000 mGy.

© 2017 Elsevier B.V. All rights reserved.

1. Introduction

Phosphor materials have been used to measure ionizing radiations [1]. These phosphors are called scintillators or dosimeters depending on the applications and luminescence phenomena involved. Scintillators convert radiations to numerous low energy photons immediately. Subsequently, the photons from the scintillators are converted to electrons by photodetectors such as photomultiplier tubes (PMTs) in general. Among scintillation properties, high light yield and short decay time are particularly important in practical applications. In contrast, the dosimeters absorb, accumulate and store incident radiation energy, and then the stored energy is released in a form of light emission by external stimulation of heat (thermally-stimulated luminescence, TSL) or light (optically-stimulated luminescence, OSL). Common examples of TSL and OSL dosimeters are LiF:Ti, Mg [2] and Al$_2$O$_3$:C [3], respectively, and they are used for personal dose monitorings. For the latter applications, the effective atomic number (Z_{eff}) should be close to that of biological tissue ($Z_{eff} = 7.51$) because interactions of ionizing radiation with matter strongly depends on the material

compositions. Furthermore, a good linear response against the incident radiation dose is also an important property. In addition to these important properties for applications, it has been of great scientific interest that luminescence properties of scintillation and dosimeter responses are complimentarily related [4,5]. Therefore, it is important to investigate both scintillation and dosimeter properties together for better understandings of ionizing radiation induced luminescence phenomena.

So far, bulk inorganic solids of single crystal and glass have been mainly used as scintillator and dosimeter because of their high optical qualities. However, transparent ceramics have been of great interest thanks to the recent advancement of sintering technologies which enable us to make ceramics with high optical transparency. Transparent ceramics have some industrial advantages such as higher mechanical strength, higher uniformity and lower fabrication cost compared with single crystals. In addition, transparent ceramics show improved properties of radiation induced luminescence in comparison with those of the single crystal form [6,7]. Furthermore, we have recently reported that non-doped MgF$_2$ transparent ceramic shows better dosimeter properties than those of single crystal [8].

MgF$_2$ has the rutile structure with space group D_{4h}^{14}, and the unit cell is simple tetragonal and contains six ions [9,10]. MgF$_2$ is one of the promising materials for dosimetry applications as it has the

* Corresponding author.
E-mail address: nakamura.fumiya.nz9@ms.nasit.jp (F. Nakamura).

effective atomic number of $Z_{eff} = 10.46$ which is close to biological tissue. For scintillation detectors, such an intermediate mass materials can be applicable in the charged particle detectors [11]. Therefore, scintillation, TSL and optical properties of MgF_2 have been intensively investigated [12—20]. In the past studies, some rare earth and transitional metal ions were doped to improve the luminescent properties. Ce^{3+} is well-known dopant and characterized by the high emission intensity and short decay time around several tens of nanoseconds due to the 5d-4f transitions [21], and some fluorides doped with Ce^{3+} such as CaF_2 and $LiCAF_6$, used in practical applications, show intense light emission [21,22]. However, to the best of our knowledge, despite the large number of earlier researches and advantages of MgF_2 as a host material and Ce ion as an activator, we found only one article regarding MgF_2 doped with Ce reporting only the TSL and radio-luminescence (RL) properties in the nanocrystalline form [18]. Other radiation-induced luminescence properties (e.g. decay time, afterglow and OSL) in Ce doped MgF_2 have not been reported in any other material forms. In order to achieve high detection efficiency of radiation, a bulk form with high optical transparency is essential since interaction probabilities of the ionizing radiations with matter simply depend on the volume of phosphor, and transparent matrix is beneficial as scintillation, TSL and OSL photons can be collected by photodetectors efficiently.

The aim of this research is to synthesize MgF_2 transparent ceramics doped with Ce^{3+} by spark plasma sintering (SPS) and investigate the optical, scintillation and dosimeter properties. SPS is a new sintering process that is characterized by a rapid consolidation rate, and it has been used to fabricate transparent ceramics [23—30]. In addition, SPS is generally performed in a high reductive atmosphere, so it can increase the defect concentration and is expected to enhance storage luminescence properties [8,31].

2. Experimental

Samples of MgF_2:Ce transparent ceramics with different concentrations of Ce were synthesized by SPS technique using Sinter Land LabX-100 in vacuum. The MgF_2 and CeF_3 raw powders (>99.99%; Tokuyama Corp.) were homogeneously mixed using a mortar and pestle. Here, the total mass of the mixture was 0.5 g, and the concentration of Ce varied as 0.01, 0.1 and 1 mol%. Subsequently, the mixture was loaded into a cylindrical graphite die with a hole of 10.4 mm in diameter and held between two graphite punches. Sintering was performed by applying uniaxial pressure through the graphite assembly while applying pulse current. The sintering was carried out in two steps. First, the temperature was elevated from the room temperature to 500 °C with a heating rate of 100 °C/min while applying 6 MPa pressure and then kept for 10 min. Next, the temperature was further elevated to 700 °C with a heating rate of 100 °C/min while applying 70 MPa pressure and then kept for 7 min. The temperature was observed by a K-type thermocouple attached onto the graphite die. After the sintering, the top and bottom surfaces of the sintered ceramic samples were mechanically polished using a polishing machine (MetaServ 250, BUEHLER). Subsequently, all the prepared samples were characterized in the same manner described below.

Optical in-line transmittance was measured by a spectrometer (V670, JASCO) over the spectral range of 190—2700 nm with 1 nm intervals. Quantaurus-QY (C11347, Hamamatsu Photonics) was used to measure PL emission and excitation spectra as well as quantum yield. Quantaurus-τ (C11367, Hamamatsu Photonics) was used to evaluate PL decay profiles.

X-ray induced scintillation spectrum was measured by our original setup [32]. As the excitation source, an X-ray generator equipped with a W anode target (XRB80P&N200X4550, Spellman)

and a Be window was used, and the X-ray generator was operated with a tube voltage of 40 kV and current of 5.2 mA. The scintillation photons from the sample were guided into a spectrometer (Andor DU-420-BU2 CCD and Shamrock 163 monochromator) thorough a 2.0 m optical fiber. The CCD detector was cooled down to 193 K by a Peltier module in order to reduce the thermal noise. In order to measure X-ray induced scintillation decay time and afterglow profiles, we have used a pulse X-ray tube equipped afterglow characterization system [33]. In fast scintillation decay measurement, a different light source from that of afterglow was used. The X-ray source was supplied with the voltage of 30 kV during the measurements.

TSL glow curve of the sample was measured by a TSL reader (TL-2000, Nanogray Inc.) over the temperature range of 50—490 °C with a heating rate of 1 °C/s [34]. Prior to the measurement, the sample was irradiated by X-rays with a certain dose ranging from 0.1 mGy to 1000 mGy. In addition, the sample was held at 50 °C for 5 min before starting the glow curve measurement. In order to measure TSL spectra, the TSL emission was collected by an optical fiber to guide into a spectrometer (QE Pro, Ocean Optics) while the sample was heated with a heating rate of 1 °C/s on a ceramic heater system (SCR-SHQ-A, Sakaguchi). OSL was evaluated under 540 nm stimulation by a spectrofluorometer (FP8600, JASCO). OSL decay profiles were also measured by FP8600 by monitoring the emission intensity at 320 nm during stimulation at 540 nm with constant intensity.

3. Results and discussion

3.1. Sample

Fig. 1 shows a picture of MgF_2:Ce transparent ceramic samples used in this research. The samples are transparent that the black lines on the back of the samples can be seen. The thicknesses of the samples were ~0.5 mm. In-line transmittance spectra of the MgF_2:Ce transparent ceramic samples are represented in Fig. 2. The transmittance of the samples decreased as the Ce concentration increased although the thicknesses were almost the same. This trend can be explained by increasing scattering centers.

3.2. Photoluminescence

Fig. 3 (a) shows the PL excitation/emission contour graph of MgF_2:1%Ce transparent ceramic sample as an example, and Fig. 3 (b) shows PL spectra of 0.01, 0.1 and 1% Ce-doped MgF_2 under

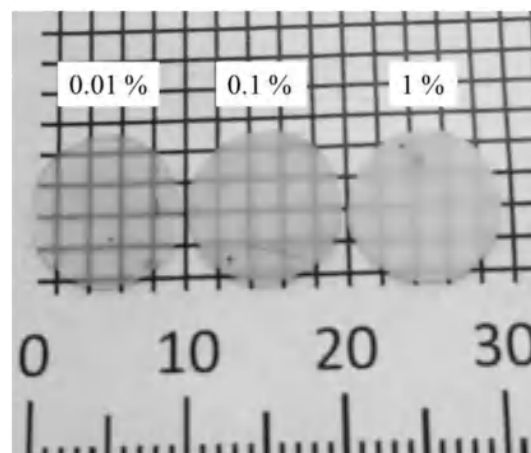**Fig. 1.** Synthesized MgF_2 transparent ceramics doped with Ce^{3+} (0.01, 0.1 and 1%).
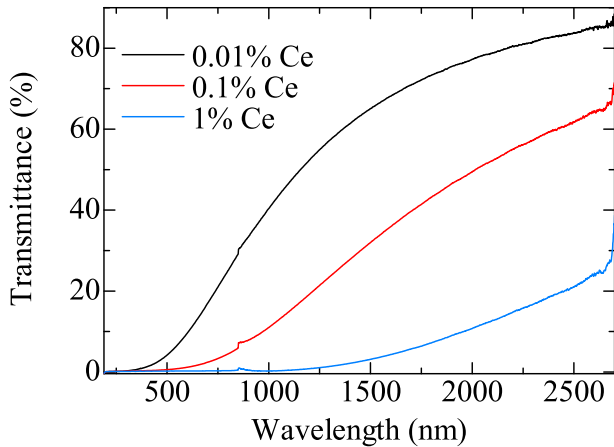
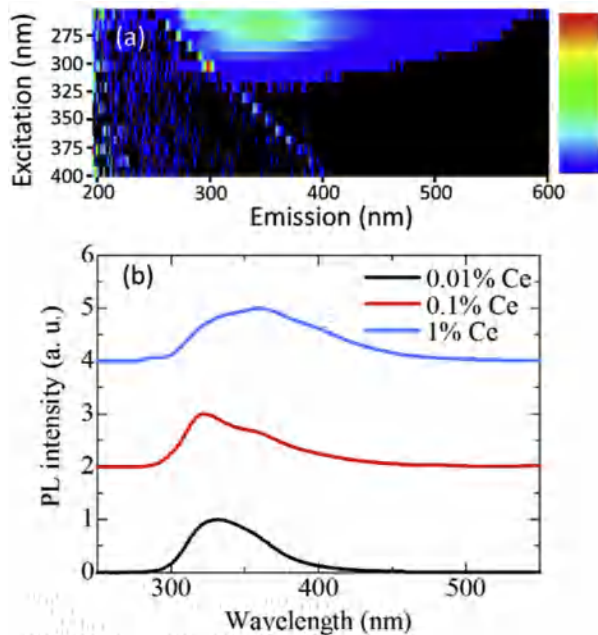**Fig. 2.** Transmittance spectra of MgF$_2$:Ce transparent ceramic samples.

Fig. 3. PL emission and excitation map of MgF$_2$:1%Ce transparent ceramic sample (a) and PL spectra of 0.01, 0.1 and 1% Ce-doped MgF$_2$ transparent ceramics under excitation at 280 nm (b).

Fig. 4. PL decay profiles of MgF$_2$:Ce transparent ceramic samples. The monitored emission wavelength were 320 (top) and 370 nm (bottom) while the excitation wavelength was 280 nm.

280 nm excitation. Under excitation at 280 nm, emission peaks were observed around 320 and 360 nm due to the 5d-4f transitions of Ce^{3+}. The energy difference between the two peaks is 3400 cm^{-1}. The value is slightly larger than the typical energy difference between $^2F_{7/2}$ and $^2F_{5/2}$ of Ce^{3+} (2000 - 2800 cm^{-1} in LaF$_3$:Ce^{3+}) [35]. In addition, it should be mentioned that there is big ionic radius difference between Mg^{2+} (0.66 Å) and Ce^{3+} (1.034 Å), so there would be some Ce^{3+} that exist as interstitial atoms in the samples. So, two PL peaks may be attributed to the 5d-4f transitions of Ce^{3+} located at different sites such as Mg^{2+} site and interstitials. Since nondoped MgF$_2$ transparent ceramics prepared in the same manner does not show such emissions [8], the origins of these emissions were attributed to Ce^{3+} ions. The intensity ratio of the peak around 320 nm to the one around 360 nm decreased with an increase in the concentration of Ce due to an overlap between the 4f-5d absorption band of Ce and a portion of emission peak at shorter wavelengths. The quantum yields of the 0.01, 0.1 and 1% Ce-
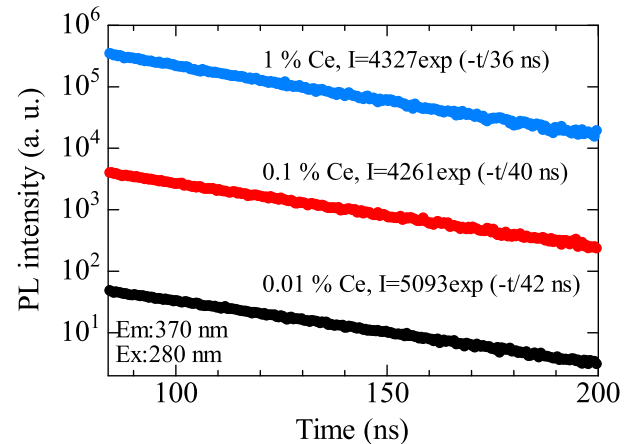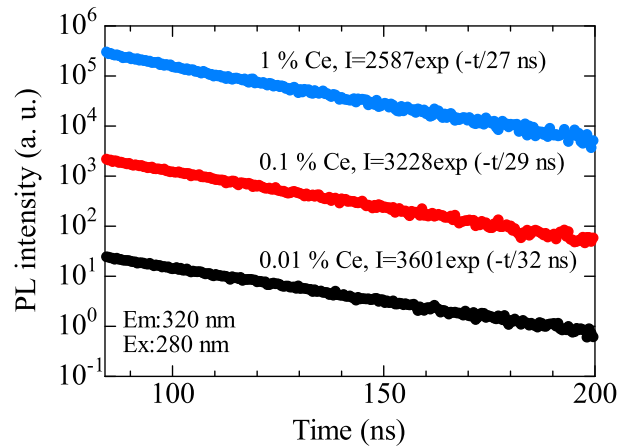
doped samples were 11, 28 and 40%, respectively. The quantum yields increased as the concentration increased.

Fig. 4 represents PL decay profiles of the MgF$_2$:Ce transparent ceramic samples. The monitored emission wavelength of the top and bottom were 320 and 360 nm, respectively. The excitation wavelength was 280 nm, which was the shortest excitation wavelength available on the instrument. The decay curves monitored at both 320 nm and 360 nm were fitted by single exponentially function. The derived decay time of the 0.01, 0.1 and 1% Ce-doped samples at 320 nm were 32, 29 and 27 ns, respectively, while 42, 40 and 36 ns for the 360 nm emission, respectively. All the decay constants were in the typical range for the 5d-4f transitions of Ce^{3+} in fluoride materials [21]. In addition, the decay times became shorter as the Ce concentration increased. The decay times were different between the peaks around 320 and 360 nm. These results supported our suggestion that the two PL peaks are due to the 5d-4f transition of Ce^{3+} at different sites.

3.3. Scintillation properties

X-ray induced scintillation spectra of MgF$_2$:Ce transparent ceramic samples are represented in Fig. 5. A broad emission which consists of several peaks was observed over 300−600 nm. The origin of the peak around 380 nm is attributed to the host because it was also observed in non-doped MgF$_2$ transparent ceramic [8]. In addition, from the results of the PL, the peaks around 320 and 360 nm would be due to the 5d-4f transitions of Ce^{3+}. The
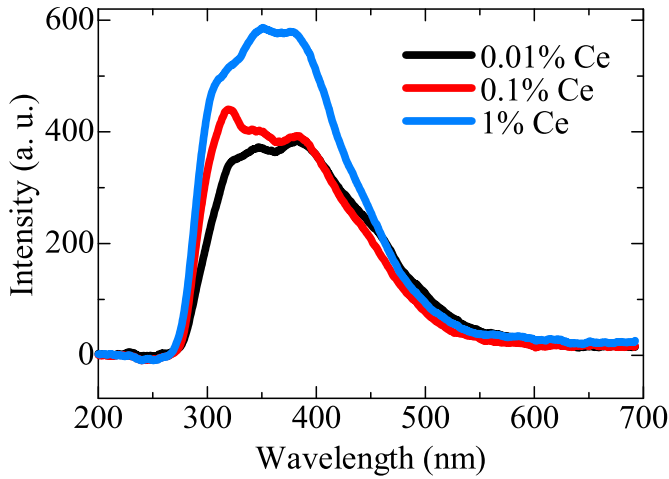
Fig. 5. X-ray induced scintillation spectra of MgF$_2$:Ce transparent ceramic samples.

intensities increased as the Ce concentration increased.

X-ray induced scintillation decay time profiles of the MgF$_2$:Ce transparent ceramic samples are shown in Fig. 6. The top and bottom figures show the decay profiles measured in short and long time ranges, respectively. In the short time range, the scintillation decay curves were fitted by single exponential function. The decay time constants of the 0.01, 0.1 and 1% Ce-doped samples measured in the shorter time range were 47, 31 and 29 ns, respectively. These values are typical for the 5d-4f transitions of Ce^{3+}. The decay times
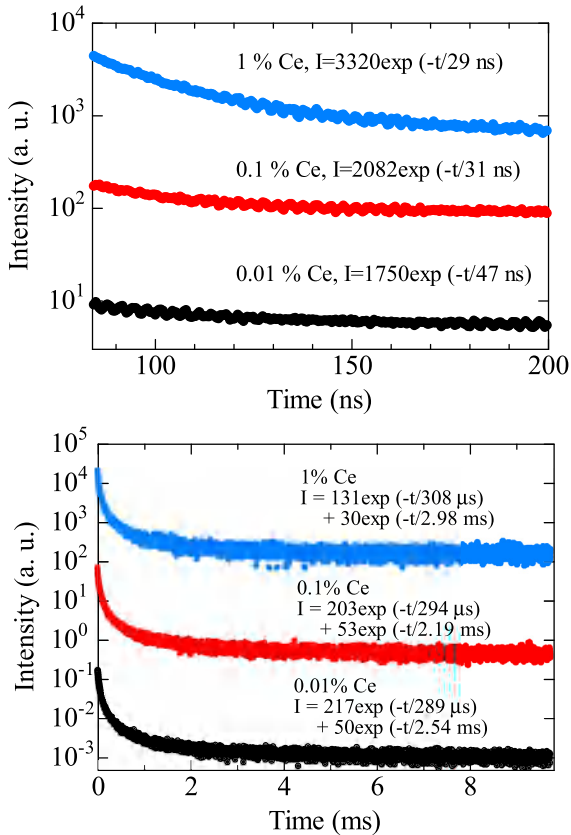

Fig. 7. Afterglow levels of MgF$_2$ transparent ceramic as a function of Ce^{3+} concentration. The inset shows afterglow profiles of the samples.

became shorter as the Ce concentration increased. Unlike PL, the scintillation decay curves were observed to consist of only single component (two for PL). The reason was that it was difficult to distinguish two components which were close to each other in both the decay time and emission wavelength. In the longer time range, the decay curves were fitted by two exponential function. The faster components of the 0.01, 0.1 and 1% Ce-doped samples were 290, 294 and 308 μs, respectively. The slower components of the 0.01, 0.1 and 1% Ce-doped samples were 2540, 2190 and 2985 μs. All the constants observed in the long range were due to the host emission around 380 nm since similar decay times were observed in the nondoped sample [8].

Afterglow levels of the MgF$_2$:Ce transparent ceramic samples are represented in Fig. 7. The inset shows the afterglow profiles. Here, the afterglow level (I_{AG}) was derived by the following formula: I_{AG} ($t = 20$ ms) [%] $= 100 \times (I_2 - I_{BG})/(I_1 - I_{BG})$ where I_{BG} is the background signal, I_1 is the averaged signal intensity during X-ray irradiation, and I_2 is the signal intensity at 20 ms after the irradiation was cut off [36]. The afterglow levels of the 0.01, 0.1 and 1% Ce-doped samples were 0.33, 0.30 and 0.20%, respectively. The afterglow level slightly decreased as the Ce concentration

Fig. 6. Scintillation decay time profiles of MgF$_2$ transparent ceramic doped with different concentrations of Ce^{3+}. The top and bottom shows the profiles over the range of 0–150 ns and 0–10 ms, respectively.
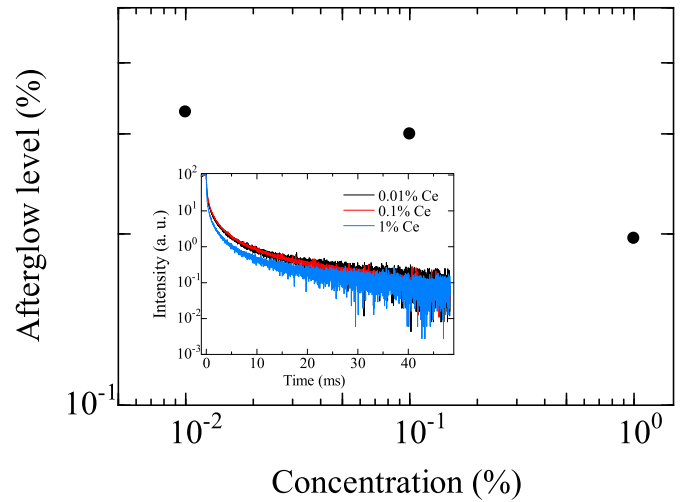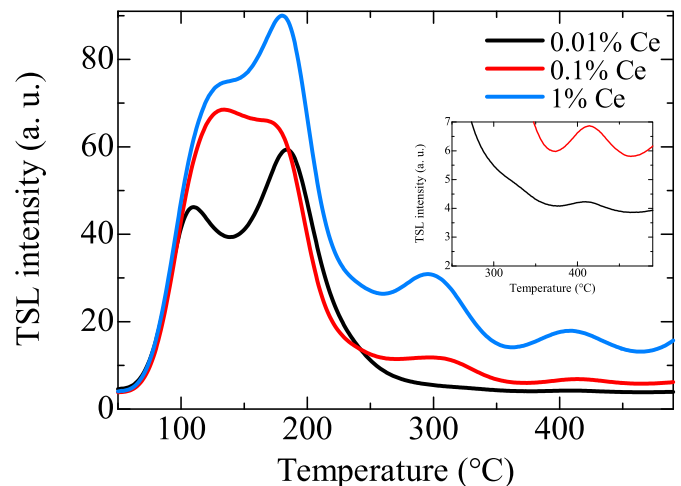

Fig. 8. TSL glow curves of MgF$_2$ transparent ceramic doped with Ce^{3+} after 1 Gy X-ray irradiation. The inset shows an enlarged view.
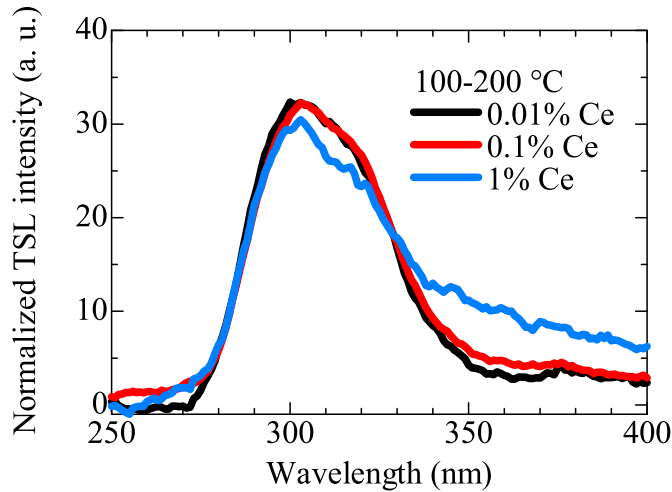
Fig. 9. TSL emission spectra of MgF_2 transparent ceramic doped with Ce^{3+} measured at 100−200 °C after 10 Gy X-ray irradiation.
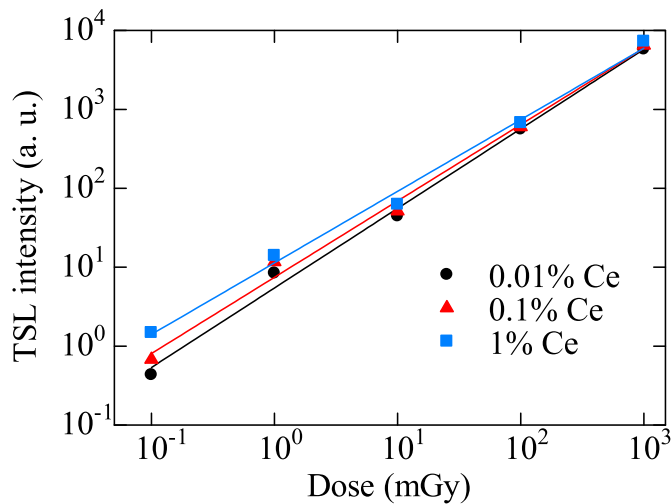

Fig. 10. TSL dose response of MgF_2 transparent ceramic doped with Ce^{3+}.
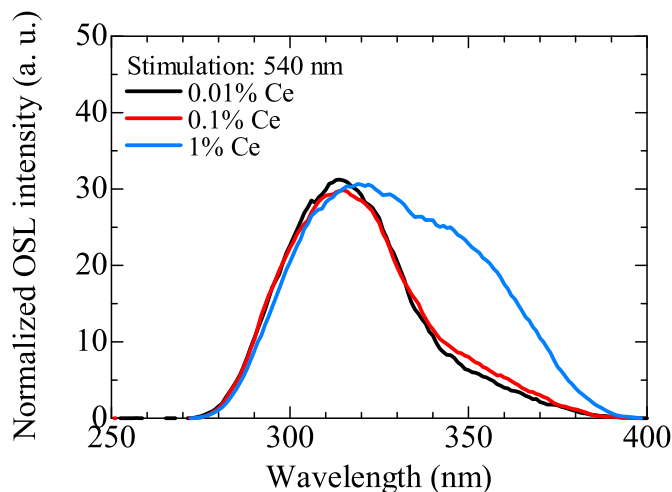

Fig. 11. OSL spectra of MgF_2:Ce transparent ceramic samples after 1 Gy X-ray irradiation.
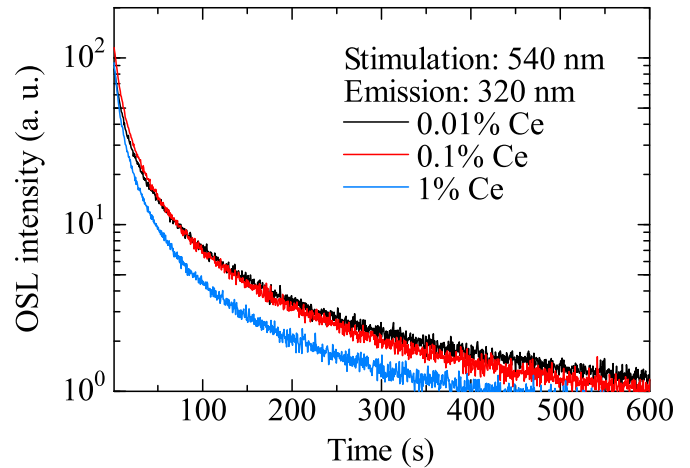

Fig. 12. OSL decay profiles of MgF_2 transparent ceramic doped with Ce^{3+}.

increased. The afterglow levels of present samples are relatively high compared with those of conventional scintillators (1−10 ppm) [33].

3.4. Dosimeter properties

TSL glow curves of MgF_2:Ce transparent ceramic samples are shown in Fig. 8. The inset enlarges the higher temperature range. There were several peaks observed in all the samples peaking around 110, 180, 300 and 400 °C. The glow peaks around 110 and 180 °C were also seen in non-doped MgF_2 transparent ceramic [8]; therefore, the peaks around 300 and 400 °C can be originated from some defect centers generated by doping with Ce^{3+}. The intensity increased with increasing the concentration of Ce^{3+}. Fig. 9 shows TSL spectra of the MgF_2:Ce transparent ceramic samples monitored at 100−200 °C. The samples showed a peak around 320 nm due to the 5d-4f transitions of Ce^{3+} while 360 nm peak appeared to be much smaller than those observed in PL and scintillation. Fig. 10 represents dose response curves of the MgF_2:Ce transparent ceramic samples. The TSL intensities were integrated values over 100−200 °C. All the samples showed a good linear response from 0.1 to 1000 mGy.

OSL spectra of the MgF_2:Ce transparent ceramic measured after X-ray irradiation (1 Gy) are shown in Fig. 11. It should be stressed here that this is the first report showing OSL in Ce-doped MgF_2. The stimulation wavelength was 540 nm. The OSL emission consists of mainly two bands peaking around 320 and 360 nm due to the 5d-4f transitions of Ce^{3+}, but the 360 nm peak was much smaller than those observed in PL and scintillation. With increasing the Ce concentration, the 360 nm peak seems to increase. If we assume that the possible origins of 320 and 360 nm peaks are Ce^{3+} in Mg^{2+} sites and interstitials, the origin of the 360 nm peak may corresponds to the Mg^{2+} sites since generally it is difficult for rare earth ions to substitute the Mg^{2+} site due to large difference of ionic radii and charge imbalance. Fig. 12 shows the OSL decay curves of the MgF_2:Ce transparent ceramic samples monitored at 320 nm under 540 nm stimulation after X-ray irradiation (1 Gy). Each decay curve can be approximated by a second-order exponential decay function, suggesting that there were at least two detrapping processes involved. The faster and slower decay constants of the 0.01, 0.1 and 1% Ce-doped samples were 12.5, 11.6 and 9.4 s and 88.2, 79.5 and 70.4 s, respectively. The values became smaller with the increase of the Ce concentration.

4. Conclusions

In this work, we have developed MgF$_2$:Ce transparent ceramics with varying doping concentrations of Ce (0.01, 0.1 and 1%) by SPS and investigated the optical, scintillation and dosimeter properties. In scintillation responses, emissions due to the host and Ce^{3+} were observed. As dosimeter properties, the MgF$_2$:Ce transparent ceramics showed good TSL properties. Especially, the TSL intensities are considerably high, and it shows the linear increase with irradiation dose from 0.1 mGy to 1000 mGy. Furthermore, the MgF$_2$:Ce transparent ceramics also showed OSL as emission peaks around 320 and 360 nm due to the 5d-4f transitions of Ce^{3+} under 540 nm stimulation.

Acknowledgements

References

[1] G.F. Knoll, Radiation Detection and Measurement, fourth ed., Wiley, New York, NY, USA, 2010.

[2] M.R. Mayhugh, R.W. Christy, N.M. Johnson, Thermoluminescence and color center correlations in dosimetry LiF, J. Appl. Phys. 41 (1970) 2968–2976, http://dx.doi.org/10.1063/1.1659346.

[3] S.W.S. McKeever, Optically stimulated luminescence: a brief overview, Radiat. Meas. 46 (2011) 1336–1341, http://dx.doi.org/10.1016/j.radmeas.2011.02.016.

[4] T. Yanagida, Ionizing radiation induced emission: scintillation and storage-type luminescence, J. Lumin 169 (2016) 544–548, http://dx.doi.org/10.1016/j.jlumin.2015.01.006.

[5] T. Yanagida, Y. Fujimoto, K. Watanabe, K. Fukuda, N. Kawaguchi, Y. Miyamoto, H. Nanto, Scintillation and optical stimulated luminescence of Ce-doped CaF$_2$, Radiat. Meas. 71 (2014) 162–165, http://dx.doi.org/10.1016/j.radmeas.2014.03.020.

[6] T. Kato, G. Okada, T. Yanagida, Optical, scintillation and dosimeter properties of MgO transparent ceramic doped and single crystal, Ceram. Int. 42 (2016) 5617–5622, http://dx.doi.org/10.1016/j.ceramint.2015.12.070.

[7] T. Yanagida, H. Takahashi, T. Ito, D. Kasama, T. Enoto, M. Sato, S. Hirakuri, M. Kokubun, K. Makishima, T. Yanagitani, H. Yagi, T. Shigeta, T. Ito, Evaluation of properties of YAG (Ce) ceramic scintillators, IEEE Trans. Nucl. Sci. 52 (2005) 1836–1841, http://dx.doi.org/10.1109/TNS.2005.856757.

[8] F. Nakamura, T. Kato, G. Okada, N. Kawaguchi, K. Fukuda, T. Yanagida, Scintillation, TSL and RPL properties of MgF$_2$ transparent ceramic and single crystal, Ceram. Int. 43 (2017) 7211–7215, http://dx.doi.org/10.1016/j.ceramint.2017.03.009.

[9] R.W.G. Wyckoff, Crystal Structure, Interscience, New York, 1965.

[10] C. Jouanin, J.P. Albert, C. Gout, Band structure and optical properties of magnesium fluoride, J. Phys. 37 (1976) 595–602, http://dx.doi.org/10.1051/jphys:01976003705059500.

[11] T. Yanagida, Y. Fujimoto, M. Miyamoto, H. Sekiwa, Optical and scintillation properties of Cd-doped ZnO film 13 (2014) 1–4.

[12] O.E. Facey, W.A. Sibley, Optical absorption and luminescence of irradiated MgF$_2$, Phys. Rev. 186 (1969) 926–932, http://dx.doi.org/10.1103/PhysRev.186.926.

[13] W.A. Sibley, O.E. Facey, Color centers in MgF$_2$, Phys. Rev. 174 (1968) 1076–1082, http://dx.doi.org/10.1103/PhysRev.174.1076.

[14] K. Tanimura, N. Itoh, Lattice instability at excited states of the self-trapped excitons in MgF$_2$, J. Appl. Phys. 69 (1991) 7831, http://dx.doi.org/10.1063/1.347514.

[15] M. Secu, S. Jipa, C.E. Secu, T. Zaharescu, R. Georgescu, M. Cutrubinis, Processes involved in the high-temperature thermoluminescence of a Mn^{2+}-doped MgF$_2$ phosphor, Phys. Status Solidi Basic Res. 245 (2008) 159–162, http://dx.doi.org/10.1002/pssb.200743108.

[16] B.C. Hong, K. Kawano, Luminescence studies of the rare earth ions-doped CaF$_2$ and MgF$_2$ films for wavelength conversion, J. Alloys Compd. 408–412 (2006) 838–841, http://dx.doi.org/10.1016/j.jallcom.2005.01.133.

[17] R.T. Williams, C.L. Marquardt, J.W. Williams, M.N. Kabler, Transient absorption and luminescence in MgF$_2$ following electron pulse excitation, Phys. Rev. B 15 (1977) 5003–5011, http://dx.doi.org/10.1103/PhysRevB.15.5003.

[18] L.G. Jacobsohn, A.L. Roy, C.L. McPherson, C.J. Kucera, L.C. Oliveira, E.G. Yukihara, J. Ballato, Rare earth-doped nanocrystalline MgF$_2$: synthesis, luminescence and thermoluminescence, Opt. Mater. (Amst) 35 (2013) 2461–2464, http://dx.doi.org/10.1016/j.optmat.2013.06.045.

[19] P.S. Senanayake, J.P.R. Wells, M.F. Reid, G. Berden, A. Meijerink, R.J. Reeves, Electron trap liberation in MgF$_2$ doped with Yb^{2+} using a two-color excitation experiment, Appl. Phys. Lett. 100 (2012) 041902, http://dx.doi.org/10.1063/1.3678630.

[20] R.F. Blunt, M.I. Cohen, Irradiation-induced color centers in magnesium fluoride, Phys. Rev. 153 (1967) 1031–1038, http://dx.doi.org/10.1103/PhysRev.153.1031.

[21] C.W.E. van Eijk, J. Andriessen, P. Dorenbos, R. Visser, Ce^{3+} doped inorganic scintillators, Nucl. Inst. Methods Phys. Res. A 348 (1994) 546–550, http://dx.doi.org/10.1016/0168-9002(94)90798-6.

[22] T. Yanagida, A. Yoshikawa, Y. Yokota, S. Maeo, N. Kawaguchi, S. Ishizu, K. Fukuda, T. Suyama, Crystal growth, optical properties, and α-ray responses of Ce-doped LiCaAlF$_6$ for different Ce concentration, Opt. Mater. (Amst) 32 (2009) 311–314, http://dx.doi.org/10.1016/j.optmat.2009.08.007.

[23] F. Nakamura, T. Kato, G. Okada, N. Kawaguchi, K. Fukuda, T. Yanagida, Scintillation and dosimeter properties of CaF$_2$ transparent ceramic doped with Eu^{2+}, Ceram. Int. 43 (2017) 604–609.

[24] T. Kato, G. Okada, K. Fukuda, T. Yanagida, Development of BaF$_2$ transparent ceramics and evaluation of the scintillation properties, Radiat. Meas.. In press.

[25] T. Kato, G. Okada, T. Yanagida, Dosimetric properties of Y-doped MgO transparent ceramics, Radiat. Meas.. In press.

[26] T. Kato, G. Okada, T. Yanagida, Dosimeter properties of MgO transparent ceramic doped with C, Radiat. Meas. 92 (2016) 93–98.

[27] T. Kato, G. Okada, T. Yanagida, Optical, scintillation and dosimeter properties of MgO transparent ceramic and single crystal, Ceram. Int. 42 (2016) 5617–5622.

[28] T. Kato, G. Okada, T. Yanagida, Optical, scintillation and dosimeter properties of MgO translucent ceramic doped with Cr^{3+}, Opt. Mater 54 (2016) 134–138.

[29] T. Kato, G. Okada, T. Yanagida, Optical, scintillation and dosimeter properties of MgO transparent ceramic doped with Mn^{2+}, J. Ceram. Soc. Jpn. 124 (2016) 559–563.

[30] T. Kato, G. Okada, T. Yanagida, Dosimeter properties of CaO transparent ceramic prepared by the SPS method, J. Mater. Sci. Mater. Electron. 28 (2017) 7018–7023.

[31] F. Nakamura, T. Kato, G. Okada, N. Kawaguchi, K. Fukuda, T. Yanagida, Scintillation and dosimeter properties of CaF$_2$ translucent ceramic produced by SPS, J. Eur. Ceram. Soc. 37 (2017) 1707–1711.

[32] T. Yanagida, K. Kamada, Y. Fujimoto, H. Yagi, T. Yanagitani, Comparative study of ceramic and single crystal Ce:GAGG scintillator, Opt. Mater. (Amst) 35 (2013) 2480–2485, http://dx.doi.org/10.1016/j.optmat.2013.07.002.

[33] T. Yanagida, Y. Fujimoto, T. Ito, K. Uchiyama, K. Mori, Development of X-ray-induced afterglow characterization system, Appl. Phys. Express 7 (2014) 8–11, http://dx.doi.org/10.7567/APEX.7.062401.

[34] T. Yanagida, Y. Fujimoto, N. Kawaguchi, S. Yanagida, Dosimeter properties of AlN, J. Ceram. Soc. Jpn. 121 (2013) 988–991, http://dx.doi.org/10.2109/jcersj2.121.988.

[35] G.H. Dieke, H.M. Crosswhite, B. Dunn, Emission spectra of the doubly and triply ionized rare earths, J. Opt. Soc. Am. 2 (1963) 675–686, http://dx.doi.org/10.1364/JOSA.51.000820.

[36] Nihon Kessyo Kogaku Co., Ltd. http://nk-k.co.jp/products/from-application/scintillator/scinti-a/, 2016 (accessed March 28, 2017).